Surface-regulated triangular borophene as Dirac-like materials from density functional calculation investigation*

Wenyu Fang(方文玉)[1], Wenbin Kang(康文斌)[1,2], Jun Zhao(赵军)[1,2,†], and Pengcheng Zhang(张鹏程)[1,‡]

[1] School of Public Health and Management, Hubei University of Medicine, Shiyan 442000, China
[2] Hubei Biomedical Detection Sharing Platform in Water Source Area of South to North Water Diversion Project, Shiyan 442000, China

(Received 21 May 2020; revised manuscript received 11 June 2020; accepted manuscript online 12 June 2020)

By applying the first principles calculations combined with density functional theory (DFT), this study explored the optical properties, electronic structure, and structure stability of triangular borophene decorated chemically, B_3X (X = F, Cl) in a systematical manner. As revealed from the results of formation energy, phonon dispersion, and molecular dynamics simulation study, all the borophene decorated chemically were superior and able to be fabricated. In the present study, triangular borophene was reported to be converted into Dirac-like materials when functionalized by F and Cl exhibiting narrow direct band gaps as 0.19 eV and 0.17 eV, separately. Significant light absorption was assessed in the visible light and ultraviolet region. According the mentioned findings, these two-dimensional (2D) materials show large and wide promising applications for future nanoelectronics and optoelectronics.

Keywords: triangular borophene, dirac material, electronic structure, first-principles calculation

PACS: 63.20.dk, 73.22.–f, 78.20.Bh, 78.20.Ci **DOI:** 10.1088/1674-1056/ab9bff

1. Introduction

Graphene[1] was initially reported by Novoselov *et al.* in 2004. Even since then, its distinctive planar structure and physical properties (*e.g.*, ultra-high carrier mobility and quantum spin Hall effect)[2] have aroused much attention. The mentioned special physical properties are primarily attributed to the Dirac cone in the electronic structure of graphene, thereby producing graphene massless fermions;[3] as a result, extremely high carrier mobility is achieved. The two-dimensional (2D) material class has been progressively broadened,[4–6] covering group-III compounds (*e.g.*, borophene,[7] aluminum[8]), group-IV compounds (*e.g.*, graphene,[9] silicene,[10] germanene,[11] stanene[12]), and group-V compounds (*e.g.*, 2D black phosphorus,[13] arsenene,[14] antimonene[15]); in the meantime, some other systems have been identified as well.[16] Note that the group-IV 2D materials (*e.g.*, arsenene[17]) can be transformed into Dirac materials when undergoing surface halogenation,[18] hydrogenation, or hydroxyl modification.[19] Nevertheless, graphene acting as the only Dirac material has been demonstrated in experiment. As a result, novel 2D materials have been explored extensively to develop more graphene-like materials. Since the successful synthesis of orthorhombic monolayer borophene, and Dirac cones in established borophene have received theoretical and experimental examination,[20] borophene[21] has aroused widespread interest. Before this effort, Tang and Ismail-Beigi,[22] *et al.* proposed two novel boron sheets consisting of triangular and hexagonal motifs. As revealed from the description of electron bonding images, as well as the analysis of chemical bonds, the hexagonal and triangular boron lattices can lead to the formation of graphene-like honeycomb structures under stable boron lattices.

In the present study, a triangular boron lattice was constructed, and a more electronegative atom X (X = F, Cl) was used to transfer electrons from the boron lattice. Then, a more stable 2D structure was formed, which is termed as B_3X (X = F, Cl) nanofilm. In accordance with the calculation method of density functional theory (DFT), two novel 2D Dirac-like materials, namely, B_3F and B_3Cl were reported, exhibiting high dynamic and thermal stability; these materials could be demonstrated by phonon calculation, dynamics simulations, and elastic constants. Note that the band structures of B_3F and B_3Cl followed Dirac materials at GGA + PBE. Their energy gaps reached 0.19 eV and 0.17 eV at HSE06, respectively, suggesting that they were Dirac-like materials. Moreover, all modified borophenes could significantly absorb visible light and ultraviolet region, suggesting their high application potential for next generation optoelectronic devices.

2. Computational methods

All the calculating processes here were achieved with the plane-wave-based CASTEP.[23] The exchange–correlation energy was expressed by the generalized gradient approximation (GGA) in the Perdew–Burke–Ernzerhof (PBE)[24] func-

*Project supported by the National Natural Science Foundation of China (Grant No. 11947006) and the Cultivating Project for Young Scholar at Hubei University of Medicine, China (Grant No. 2018QDJZR22).

†Corresponding author. E-mail: stzhao@163.com
‡Corresponding author. E-mail: pengchzhang@163.com

tional. The core electrons were substituted by the projector augmented-wave (PAW) pseudopotentials. The Heyd–Scuseria–Ernzerhof (HSE06)[25] screened hybrid functional was adopted for the calculation of B_3X band structures to narrow the underestimated band gaps in GGA-PBE.[26,27] The valence electron configurations involved in the calculations here included: B($2s^2 2p^1$), F($2s^2 2p^5$), and Cl($3s^2 3p^5$). For the optimization of geometric structure, the convergence criteria for total energy were set to 5.0×10^{-6} eV, and Hellmann–Feynman forces on the respective atom were below 0.01 eV/Å in the respective direction. A $15 \times 15 \times 1$ k-point grid yielded following the scheme of Monkhorst–Pack was taken to achieve Brillouin zone sampling, and a kinetic energy cutoff of the plane wave basis was taken as 500 eV. For limiting the artificial interaction between adjacent layers, a 20-Å vacuum slab was added to all the 2D materials following the z-axis direction. By applying norm-conserving pseudopotentials and finite difference method, the phonon spectra were calculated. To ascertain the thermal stability of the structures, molecular dynamics simulations with a $3 \times 3 \times 1$ supercell were conducted, in which the NVT canonical ensemble was adopted.

3. Results and discussion

3.1. Crystal structure and stability

Borophene has two common structures, namely, hexagonal and triangular boron lattices, each of which exhibits their own defects. The hexagonal boron lattice exhibits low stability for the lack of electrons, while the triangular boron lattice exhibits low stability for electrons oversupply.[28] To develop a stable 2D borophene structure, a mixture of hexagonal and triangular boron lattices was employed. For insufficient electrons, a smaller electronegative metal atom is usually introduced to input electrons, thereby making hexagonal borophene exhibit higher stability.[29] Accordingly, two 2D structures were designed based on triangular boron lattices, termed as B_3X (X = F, Cl). To ascertain the rationality of the design idea, here, phonon spectrum calculation and AIMD simulation were conducted to demonstrate its dynamic and thermal stability. Moreover, its electronic structure and other physical properties were analyzed specifically.

The design here complies with the structure of graphene (as shown in Fig. 1). Since B atom has only three valence electrons, while C atom has four; the graphene-like honeycomb structure (hexagonal lattice) exhibits low stability. It is therefore suggested that compared with graphene, the hexagonal honeycomb boron lattice lacks two electrons in its six-member ring, so an atom capable of providing two electrons should be introduced. It was decorated with a B atom in the center of a six-membered boron ring. In such an optimized structure, it was reported that the introduced B atom tended to lie in the center of the planar six-member boron ring, thereby revealing that the optimized structure was flat, corresponding to the triangular boron lattice. However, B atom covers three valence electrons. Triangular borophene consists of an extra electron compared with graphene in each of its six membered rings, lowering its stability, which can be confirmed by phonon spectrum calculation (Fig. 2). It exhibits a high imaginary frequency, so its structure exhibits low stability. To transfer the extra electrons from the triangular borophene, an atom being more electro-negative than boron was chosen to modify the B atom at the center of the six-membered ring. The objective of such effort was to ensure that the boron lattice has the identical number of valence electrons as graphene, as an attempt to maintain the stability of the system. The selection principle of the modified atom was ascertained by electronegativity, electron number, and atomic radius. In the triangular boron lattice, six-membered boron covers one electron more than graphene's six-membered carbon ring. For this reason, if modified atoms are more electro-negative than B atoms, it is able to capture one electron only, and with the appropriate atomic radius to avoid destroying the boron lattice. It is generally known that halogens are very electronegative, and F (64 Å) and Cl (99 Å) have atomic radius close to that of B (77 Å). Accordingly, F and Cl were taken as modified atoms, and the designed structure was termed as B_3X (X = F, Cl). In Fig. 1, B atom modified by F or Cl moved towards the 2D material surface perpendicularly to the slab. Thus, the modified atoms led to the destruction of the original planar structure of the triangular borophene, while a buckling height was identified on B_3X surface. After optimization, the folded modified boron lattice had clearly higher formation energy (absolute value) and greater chemical stability compared with the ideal B_3X triangular boron, since the structure with the maximal formation energy would be taken during the optimization, the structure would exhibit higher stability.

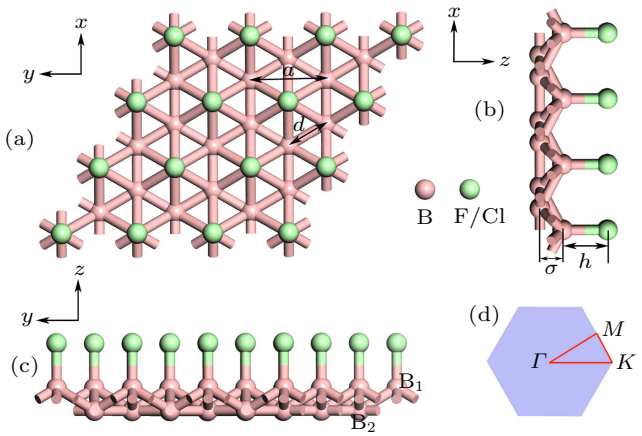

Fig. 1. The optimized geometric structures for the B_3X (X = F, Cl) and the 2D Brillouin zone (BZ) of the monolayers exhibiting high symmetry k-points.

As suggested from the optimization results, all the optimized structures still maintained the triangular lattice, whereas

the boron lattice no longer maintained the original planar structure, and B_3X buckling took place. The optimized structure parameters are listed in Table 1. The boron atom in the six-membered ring was labeled as B_1, and the boron atom in the center of the six-membered ring was marked as B_2, while the modified atoms were represented by X. In Table 1, the lattice constant is expressed by a, the bond length between B_1 and B_2 atoms is denoted as l, and the bond length between two adjacent B_1 atoms in the identical layer is indicated as d, the bond length between B_2 and modified atom X is denoted as h, σ is bulking height, and the formation energy is represented by E_f. According to the results, since the atomic radius of F (0.64 Å) was smaller than that of Cl (0.99 Å), the a, d, and h of B_3F were smaller than those of B_3Cl, while σ was down-regulated. Moreover, since F (10.41) atom and Cl (8.30) atom were noticeably more electro-negative than B (4.29) atom, the valence electron environment of B_2 atom varied; as a result, a slight difference occurred in σ terms. For 2D materials, phonon curves have been generally adopted to analyze their dynamic stability, so the phonon curves of B_3X were calculated (Fig. 3). The phonon curves of B_3F are suggested with an imaginary frequency at the Γ spot, whereas it is relatively thin. It can be considered as attributed to the calculation error and ignorable. The phonon curves of B_3Cl exhibit no virtual frequency, suggesting that they all exhibit high dynamic stability.

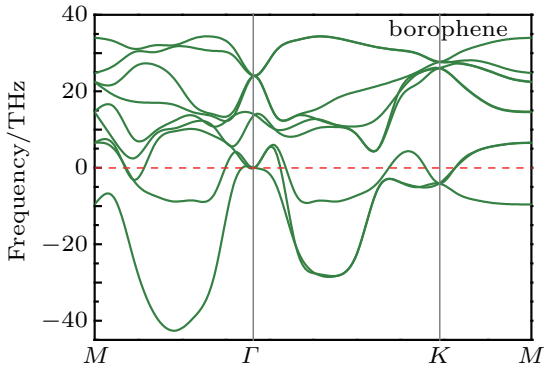

Fig. 2. Phonon dispersion of triangular borophene.

Table 1. Calculated lattice constant a, bond lengths d, h, buckling height σ, and binding energy E_f (marked in Fig. 1) as well as electronic energy band gaps (based on both PBE and HSE06 functionals) of all chemically decorated triangular borophene.

Materials	a/Å	d/Å	h/Å	σ/Å	E_f/eV	PBE/eV	HSE06/eV
B_3F	2.88	1.66	1.35	0.90	−5.08	0	0.19
B_3Cl	2.97	1.71	1.75	0.89	−2.14	0	0.17

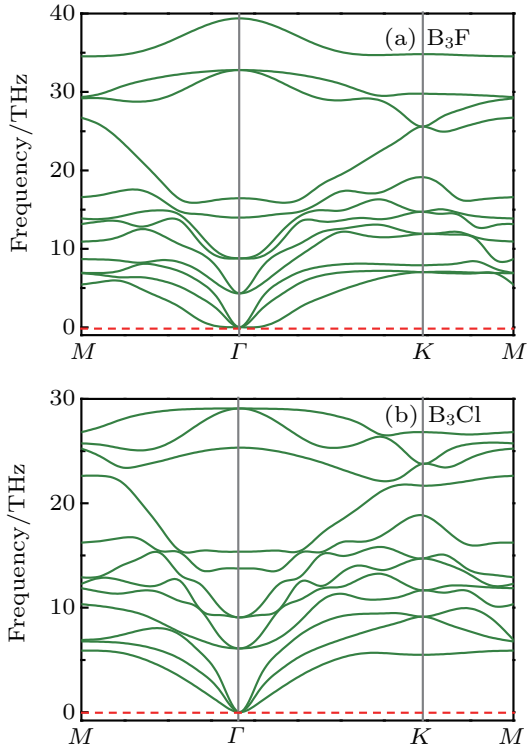

Fig. 3. Phonon dispersion of (a) B_3F and (b) B_3Cl.

AIMD simulations were further conducted to ascertain the thermal stability of B_3X, and the results are presented in Figs. 4(a) and 4(b). The total energy of these two structures fluctuated slightly when they were being annealed at 500 K for 10 ps (within 1 eV). Accordingly, B_3X could exist stably at ambient temperature, and it is feasible to fabricate these 2D materials in experiments. It is therefore confirmed that the design idea here is reasonable. These 2D borophene structure could also be built on the triangular lattice as well. To verify the relative stability of the two systems, the formation energy was calculated, as defined below[30]

$$E_f = E(B_3X) - E(B_3) - E(X), \tag{1}$$

where $E(B_3X)$, $E(B_3)$, and $E(X)$ are the total energies of the chemical decorated B_3X, the free-standing triangular borophene, and the chemical potential of the single $-X$ (X = F, Cl) group, respectively. As listed in Table 1, the formation energy of all systems is negative, demonstrating that the fabrication of these materials is an exothermic reaction. As revealed from these results, B_3X (X = F, Cl) is highly stable and can be fabricated experimentally.

Table 2. The elastic constants of all chemically decorated triangular borophene calculated by GGA + PBE.

Materials	C_{11}/GPa	C_{22}/GPa	C_{12}/GPa	C_{66}/GPa	$C_{11}C_{22}-C_{12}^2$
B_3F	110.42	110.42	14.02	48.20	22996.02
B_3Cl	109.65	109.65	36.47	36.59	10693.06

From the mechanical perspective, a stable 2D structure

should comply with the Born–Huang criteria,[31] expressed as $C_{11}C_{22}-(C_{12})^2>0$ and $C_{66}>0$, where C_{ij} denotes the elastic constant. For the hexagonal symmetry of B_3X, one naturally achieved $C_{11}=C_{22}$; the calculated results are listed in Table 2. Thus, all B_3X completely complied with the mechanical stability criterion. As indicated from all the analysis results, B_3X exhibited high dynamic, thermal, and mechanical stability as free standing 2D materials.

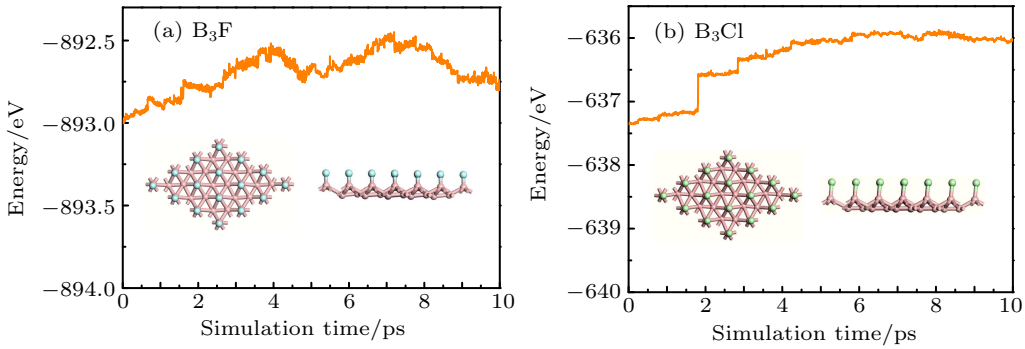

Fig. 4. Variation of the total energy in the molecular dynamics simulation at 500 K during a timescale of 10 ps for (a) B_3F and (b) B_3Cl. The insets give the top (left panel) and side (right panel) views of the atomic structure snapshots taken from the molecular dynamics simulation.

3.2. Mechanical property

To delve into the mechanical properties of B_3X, the elastic constants[32] were calculated, and subsequently the in-plane Young's modulus $Y(\theta)$ and Poisson's ratio $\upsilon(\theta)$ of B_3X were further fitted. $Y(\theta)$ and $\upsilon(\theta)$ following the in-plane θ are[33]

$$Y(\theta)=\frac{C_{11}C_{12}-C_{12}^2}{C_{11}\sin^4\theta+\left(\dfrac{C_{11}C_{12}-C_{12}^2}{C_{66}}-2C_{12}\right)\sin^2\theta\cos^2\theta+C_{22}\cos^4\theta}, \tag{2}$$

$$\upsilon(\theta)=\frac{C_{12}\sin^4\theta-\left(C_{11}+C_{22}-\dfrac{C_{11}C_{12}-C_{12}^2}{C_{66}}\right)\sin^2\theta\cos^2\theta+C_{12}\cos^4\theta}{C_{11}\sin^4\theta+\left(\dfrac{C_{11}C_{12}-C_{12}^2}{C_{66}}-2C_{12}\right)\sin^2\theta\cos^2\theta+C_{22}\cos^4\theta}. \tag{3}$$

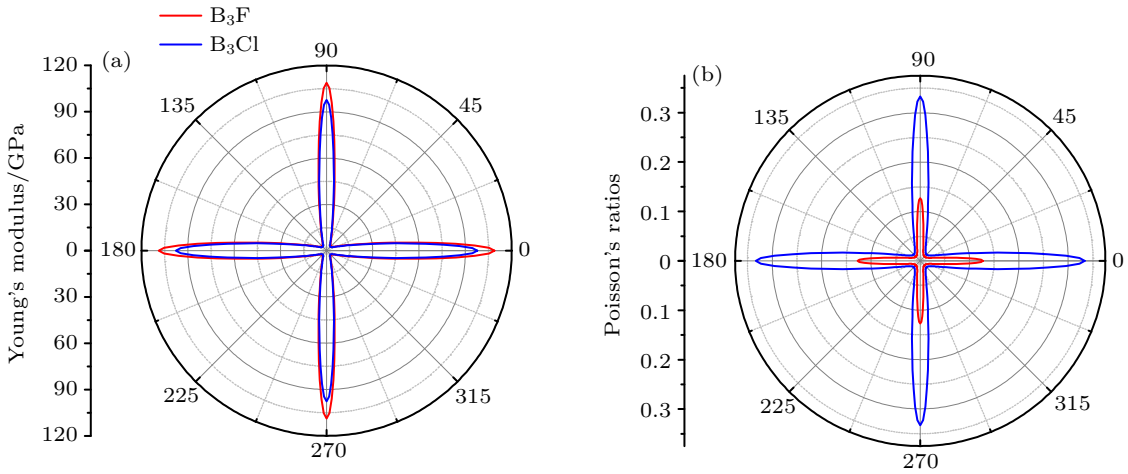

Fig. 5. Polar diagram for (a) Young's modulus and (b) Poisson's ratio of B_3X (X = F, Cl). θ is the angle with respect to the a-direction.

According to Figs. 5(a) and 5(b), the Young's modulus and Poisson's ratio of B_3X are anisotropic. The mentioned structures suggested similar mechanical responses to the identical strain from a range of directions. The Young's moduli of B_3F and B_3Cl were peaked following the axis (at $\theta=0^\circ$ and 270°), 108.64 GPa and 97.52 GPa, respectively. Compared with common 2D materials, they are significantly smaller than graphene (1.0 TPa)[34] and monolayer MoS_2 (330 GPa),[35] evidently larger than black phosphorus (41.3 GPa)[36] and comparable to 2D TnSe (101.37 GPa).[37] Accordingly, B_3F and B_3Cl exhibited large deformation–resistance flexibility in both a and b directions. For Poisson's ratio, B_3F and B_3Cl also reach their maximal values following a- and b-orientations as 0.13 and 0.33, respectively, being comparable to graphene (0.175)[38] and monolayer MoS_2 (0.25).[39] The Poisson's ratio following the diagonal direction is noticeably lower than

that of axis-direction with the minimal value of 0.012 and 0.018 for B_3F and B_3Cl, respectively.

3.3. Electronic properties

Given that the spin–orbit coupling (SOC) effect is likely to impact the electronic properties of B_3X, SOC effects were considered in all upcoming calculations of electronic structures unless otherwise stated. Through the spin polarization calculating process, the magnetic moment of all the atoms in the B_3X lattice was reported to be nearly zero. Figure 6 presents the band structure and density of states of B_3X. As shown in Figs. 6(a) and 6(b), at the PBE + SOC level, both B_3F and B_3Cl exhibited unanimously linear energy dispersion that crossed the Fermi energy at the K points; they also formed Dirac cones. Since GGA + PBE functionals underestimate the band gap on the whole,[40] the Heyd–Scuseria–Ernzerhof (HSE06) hybrid exchange–correlation functional was adopted to correct the band structure.[41,42] A lager bandgap of 0.19 eV and 0.17 eV was demonstrated by the HSE06 + SOC calculation for B_3F and B_3Cl. Note that, except for slight energy differences, HSE06 + SOC exhibited a very similar band structure to that at the PBE + SOC level. These Dirac-like band structures of B_3F and B_3Cl indicated that the band also exhibits linear dispersion and great application prospects in the future.[43] Furthermore, the valence band maximum (VBM) and conduction band minimum (CBM) of B_3F and B_3Cl were both located at K point, demonstrating that they are direct bandgap semiconductors. Moreover, according to the partial density of states (PDOS) plotted in Figs. 6(a) and 6(b), both the VBM and CBM of B_3X were dominated by B-4p orbitals, while the contribution of F-2p or Cl-3p orbitals was small. It is noteworthy that both Br and I are also halogens. What if we substitute X with them? To verify the effectiveness of this idea, the band structures of B_3Br and B_3I were also calculated (see Figs. 7(c) and 7(d)). However, the results of B_3Br and B_3I were different. According to the calculation results of both GGA + PBE + SOC and HSE06 + SOC, their energy levels generally shifted to lower energy levels, and the original Dirac cone was transferred to below the Fermi surface, and they are adopted as metal materials.

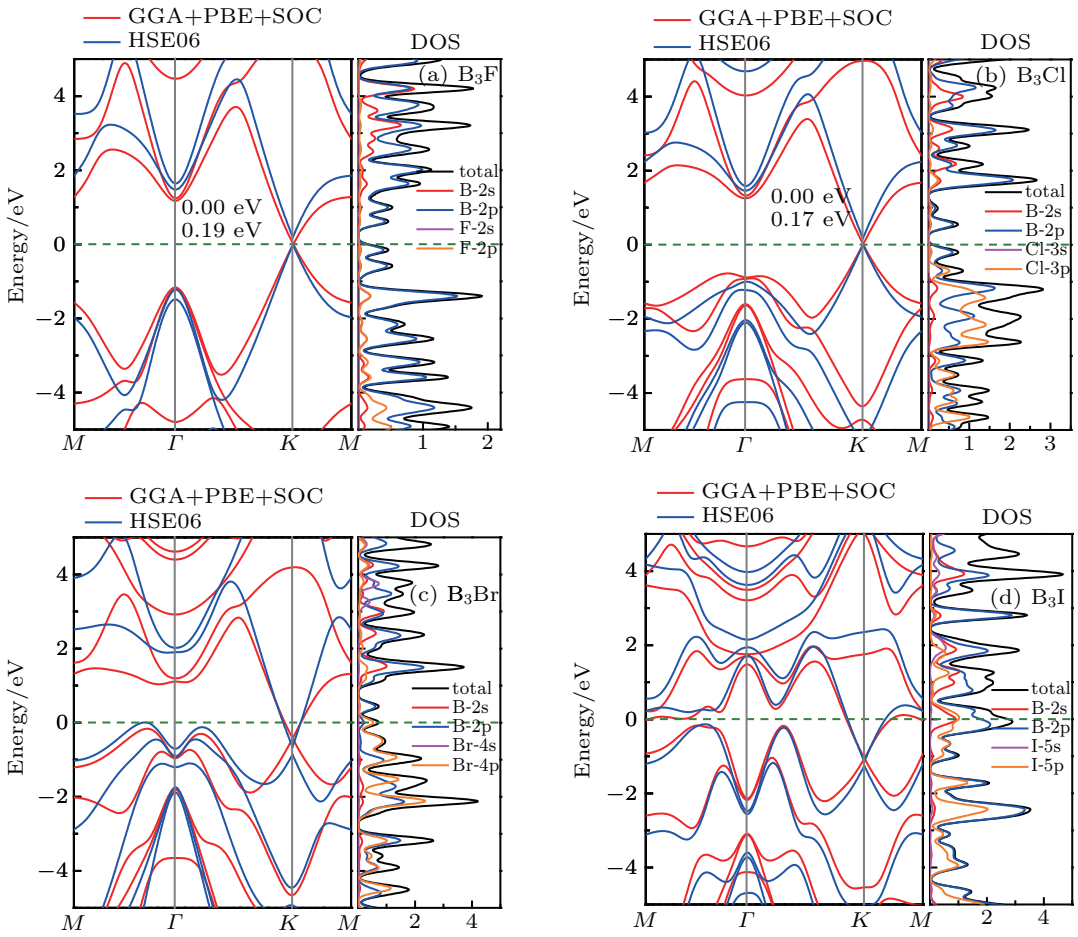

Fig. 6. Electronic band structures and density of states of (a) B_3F, (b) B_3Cl, (c) B_3Br, and (d) B_3I.

For Dirac materials, the Fermi velocity to some extent reflects the electrical conductivity, so the Fermi velocities of these two Dirac-like materials were calculated to analyze their conductivity. The Fermi velocity can be generally obtained by first order linear fitting of the band near Dirac point (K point), which is written as[44]

$$V_{\mathrm{F}} = \frac{2\pi}{h}\frac{\partial E}{\partial k}, \tag{4}$$

where h denotes Planck's constant, and $\partial E/\partial k$ indicates the gradient of the band near Dirac point. The Fermi velocities are calculated by Eq. (4). For the symmetry of the Dirac cone, the curve near the top of the valence band should be only fitted, as listed in Table 3. Fermi velocities vary with directions, demonstrating that the electrical conductivity of B_3F and B_3Cl exhibited directional anisotropy. Following $K \to \Gamma$, the Fermi velocities (at HSE06 + SOC) of B_3F and B_3Cl were 7.39×10^5 m/s and 6.54×10^5 m/s, respectively. They are close to the Fermi velocity of graphene (about 9.5×10^5 m/s),[45] demonstrating that these two systems are highly likely to act as the conducting materials.

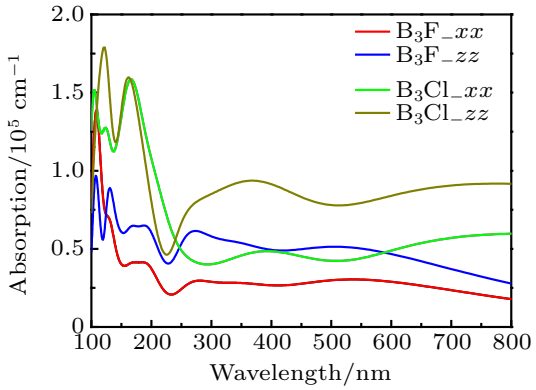

Fig. 7. Calculated in-plane and out-plane light absorption coefficients of monolayer B_3F and B_3Cl, using the screened HSE06 hybrid functional.

Table 3. Fermi velocities at the valence band top of B_3F and B_3Cl (based on both PBE and HSE06 functionals).

Direction	PBE/10^5 (m/s)		HSE06/10^5 (m/s)	
	$K \to \Gamma$	$K \to M$	$K \to \Gamma$	$K \to M$
B_3F	6.33	5.17	7.39	6.59
B_3Cl	5.62	5.14	6.54	6.25

3.4. Light harvesting

For optical properties, B_3F and B_3Cl are Dirac-like materials and exhibit a tiny energy gap, demonstrating that they could noticeably absorb infrared and visible light. Thus, the HSE06 function was adopted to calculate the absorption spectra of B_3X (X = F, Cl) in- and out-of-plane, and their optical properties were delved into. The transverse dielectric function[46,47] $\varepsilon(\omega) = \varepsilon_1(\omega) + \mathrm{i}\varepsilon_2(\omega)$ is generally employed to describe the optical properties of materials, where ω denotes the photon frequency, $\varepsilon_1(\omega)$ is the real part, and $\varepsilon_2(\omega)$ refers to the imaginary part of the dielectric function, respectively. The absorption coefficient can be calculated from[48]

$$\alpha(\omega) = \frac{\sqrt{2\omega}}{c}\left\{\left[\varepsilon_1^2(\omega) + \varepsilon_2^2(\omega)\right]^{1/2} - \varepsilon_1(\omega)\right\}^{1/2}, \tag{5}$$

where c denotes the speed of light. According to Fig. 7, the absorption coefficient of B_3X (X = F, Cl) reaches the order of 10^5 cm^{-1} and covers the wide wavelength range of visible light and ultraviolet region, suggesting the potential applications of B_3X (X = F, Cl) as efficient optical absorber materials in solar cells and photovoltaic devices.

4. Conclusion

In the present study, a novel material design method was developed, capable of stabilizing the triangular boron lattice structure by introducing a modified atom to transfer excess electrons. Thus, two new 2D materials, namely, X (X = F, Cl) atom modified single-layer triangular borophene B_3X, were constructed. As revealed from the calculated results of forming energy, phonon dispersion, molecular dynamics simulation, and elastic constant, they could exist stably, *i.e.*, the experimental synthesis is completely feasible, while our material design method is reasonable. The band structures demonstrated that B_3F and B_3Cl are Dirac materials at GGA + PBE, and the Dirac cone point is located at K point of BZ, exhibiting the energy gap of 0.19 eV and 0.17 eV at HSE06, respectively, which are Dirac-like materials. Moreover, B_3Br and B_3I were converted into metallic materials whether at GGA + PBE or HSE06. The Fermi velocities of B_3F and B3Cl monolayer reached 7.39×10^5 m/s and 6.54×10^5 m/s, respectively. Furthermore, both B_3F and B_3Cl achieved significant light absorption in the solar spectrum. These findings demonstrated that 2D B_3F and B_3Cl are likely to be future applied in nanoelectronics and optoelectronics.

Acknowledgment

Thanks for the support of National Supercomputing ShenZhen Center.

References

[1] Novoselov K S, Geim A K, Morozov S V, Jiang D, Zhang Y, Dubonos S V, Grigorieva I V and Firsov A A 2004 *Science* **306** 666
[2] Van Noorden R 2006 *Nature* **442** 228
[3] Luk'yanchuk I A and Kopelevich Y 2006 *Phys. Rev. Lett.* **97** 256801
[4] Cao M S, Wang X X, Zhang M, Shu J C, Cao W Q, Yang H J, Fang X Y and Yuan J 2019 *Adv. Funct. Mater.* **29** 1807398
[5] Fu N W, Ji C L, Yi L, Xin M Z, Xue J W, Yu F C, Jian L Chun L W, Ming L Z and Liang M M 2019 *Chin. Phys. B* **28** 047101
[6] Yan F G and Yong L 2019 *Chin. Phys. B* **28** 077104
[7] Karthikeyan J, Ranawat Y S, Murugan P, Kumar V 2018 *Nanoscale* **10** 17198
[8] Yuan J H, Yu N N, Xue K H, Miao X S 2017 *Appl. Surf. Sci.* **409** 85
[9] Hashimoto A, Suenaga K, Gloter A, Urita K and Iijima S 2004 *Nature* **430** 870
[10] Zhu Y L, Yuan J H, Song Y Q, Wang S, Xue K H, Xu M, Cheng X M and Miao X S 2019 *J. Mater. Sci.* **54** 11485
[11] Shih P H, Chiu Y H, Wu J Y, Shyu F L, Lin M F 2017 *Sci. Rep.* **7** 40600
[12] Chaudhary R P, Saxena S and Shukla S 2016 *Nanotechnology* **27** 495701
[13] Wu L, Wang J, Lu J, Liu D, Yang N, Huang H, Chu P K and Yu X F 2018 *Small* e1801405
[14] Zhang S, Yan Z, Li Y, Chen Z and Zeng H 2015 *Angew. Chem. Int. Ed. Engl.* **54** 3112
[15] Wang X, Song J and Qu J 2019 *Angew. Chem. Int. Ed. Engl.* **58** 1574

[16] Zhao Y, Li X, Liu J, Zhang C and Wang Q 2018 *J. Phys. Chem. Lett.* **9** 1815
[17] Carrete J, Gallego L J and Mingo N 2017 *J. Phys. Chem. Lett.* **8** 1375
[18] Tang W, Sun M, Ren Q, Wang S and Yu J 2016 *Appl. Surf. Sci.* **376** 286
[19] Yuan J, Xie Q, Yu N and Wang J 2017 *Appl. Surf. Sci.* **394** 625
[20] Wu R, Drozdov I K, Eltinge S, Zahl P, Ismail-Beigi S, Bozovic I and Gozar A 2019 *Nat. Nanotechnol.* **14** 44
[21] Sheng S, Wu J B, Cong X, Zhong Q, Li W, Hu W, Gou J, Cheng P, Tan P H, Chen L and Wu K 2019 *ACS Nano* **13** 4133
[22] Tang H and Ismail-Beigi S 2007 *Phys. Rev. Lett.* **99** 115501
[23] Qiu G, Xiao Q, Hu Y, Qin W, Wang D 2004 *J. Colloid Interface Sci.* **270** 127
[24] Perdew J P, Burke K and Ernzerhof M 1996 *Phys. Rev. Lett.* **77** 3865
[25] Krukau A V, Vydrov O A, Izmaylov A F and Scuseria G E 2006 *J. Chem. Phys.* **125** 224106
[26] Song Y Q, Yuan J H, Li L H, Xu M, Wang J F, Xue K H, Miao X S 2019 *Nanoscale* **11** 1131
[27] Zhen-Ye Z, Si-Qi W and Yan-Ming F 2016 *Chin. Phys. Lett.* **33** 026302
[28] Yuan J, Yu N, Xue K and Miao X 2017 *RSC Adv.* **7** 8654
[29] Fan M, Wen Y, Ye D, Jin Z, Zhao P, Chen D, Lu X, He Q 2019 *Adv. Healthc. Mater.* **8** e1900157
[30] Zhao J, Li Y and Ma J 2016 *Nanoscale* **8** 9657
[31] Fang W Y, Li P A, Yuan J H, Xue K H and Wang J F 2020 *J. Electron. Mater.* **49** 959
[32] Yu Y, Chen C L, Zhao G D, Zheng X L and Zhu X H 2014 *Chin. Phys. Lett.* **31** 106301
[33] Peng R, Ma Y, He Z, Huang B, Kou L and Dai Y 2019 *Nano Lett.* **19** 1227
[34] Lee C, Wei X, Kysar J W and Hone J 2008 *Science* **321** 385
[35] Castellanos-Gomez A, Poot M, Steele G A, Van Der Zant H S, Agrait N and Rubio-Bollinger G 2012 *Adv. Mater.* **24** 772
[36] Li L and Yang J 2017 *Nanotechnology* **28** 475701
[37] Li Y, Yu C, Gan Y, Kong Y, Jiang P, Zou D F, Li P, Yu X F, Wu R, Zhao H, Gao C F and Li J 2019 *Nanotechnology* **30** 335703
[38] Liu L, Zhang J, Zhao J and Liu F 2012 *Nanoscale* **4** 5910
[39] Kang J, Sahin H and Peeters F M 2015 *Phys. Chem. Chem. Phys.* **17** 27742
[40] Zhang D, Xiong Y, Cheng J, Chai J, Liu T, Ba X, Ullah S, Zheng G, Yan M and Cao M 2020 *Sci. Bull.* **65** 138
[41] Hua C, Sheng F, Hu Q, Xu Z A, Lu Y and Zheng Y 2018 *J. Phys. Chem. Lett.* **9** 6695
[42] Feng S Q, Li J Y and Cheng X L 2015 *Chin. Phys. Lett.* **32** 036301
[43] Weick G, Woollacott C, Barnes W L, Hess O and Mariani E 2013 *Phys. Rev. Lett.* **110** 106801
[44] Zhang Y, Kang J, Zheng F, Gao P F, Zhang S L and Wang L W 2019 *J. Phys. Chem. Lett.* **10** 6656
[45] Xu L C, Du A and Kou L 2016 *Phys. Chem. Chem. Phys.* **18** 27284
[46] Fang W Y, Zhang P C, Zhao J and Kang W B 2020 *Acta Phys. Sin.* **69** 056301 (in Chinese)
[47] Wang Y F and Li X W 2018 *Acta Phys. Sin.* **67** 116301 (in Chinese)
[48] Mogulkoc A, Mogulkoc Y, Kecik D and Durgun E 2018 *Phys. Chem. Chem. Phys.* **20** 21043